applied sciences

MDPI

Article

The Study of Multi-Stage Cold Forming Process for the Manufacture of Relief Valve Regulating Nuts

Chih-Cheng Yang [1,*] and Chi-Hsuan Liu [2]

[1] Department of Mechanical and Automation Engineering, Kao Yuan University, Kaohsiung 82151, Taiwan
[2] Graduate School of Fasteners Industry Technology, Kao Yuan University, Kaohsiung 82151, Taiwan; s0918855963@gmail.com
* Correspondence: t30043@cc.kyu.edu.tw; Tel.: +886-7-6077027

Abstract: Cold forging is widely used in many industries. Multi-stage cold forming is usually utilized in forging fasteners. In this study, numerical simulation and experimental investigations were carried out on a five-stage cold-forming process for the manufacturing of low-carbon steel AISI 1010 relief valve regulating nuts. The forming process through five stages included preparation and centering for backward extrusion, backward extrusion over die pin, upset, backward extrusion over moving punch, and piercing. The formability of the workpiece was studied, such as the effects on forming force response, maximum forming force, effective stress and effective strain distributions, metal flow patterns, and strength. A comparison of the forming forces obtained in the forming experiment with the numerical simulation results of the five-stage cold forming showed a good agreement with the trend of the forming force growth. For the maximum forming force and forming energy, the fourth stage of backward extrusion over the moving punch at the upper face was the largest among the five stages. The total maximum forming forces from the first to the fifth stages were numerically 440.9 kN and experimentally 449.4 kN, meaning the FE simulation and experimental results were in good agreement. The numerically simulated effective strain distributions were consistent with the experimentally tested hardness distributions. Highly compacted grain flow lines also resulted in higher hardness. The overall hardness of the workpiece formed by five-stage cold forming increased by 31% compared to the initial billet. The hardness of the workpiece increased with the forming stages, and the strain-hardening effect was obvious. The strength of the workpiece was significantly increased by five-stage cold forming.

Keywords: multi-stage cold forming; formability; forming force; effective stress; effective strain; hardness

check for updates

Citation: Yang, C.-C.; Liu, C.-H. The Study of Multi-Stage Cold Forming Process for the Manufacture of Relief Valve Regulating Nuts. *Appl. Sci.* **2023**, *13*, 6299. https://doi.org/10.3390/app13106299

Academic Editor: Cem Selcuk

Received: 17 April 2023
Revised: 18 May 2023
Accepted: 19 May 2023
Published: 22 May 2023

Copyright: © 2023 by the authors. Licensee MDPI, Basel, Switzerland. This article is an open access article distributed under the terms and conditions of the Creative Commons Attribution (CC BY) license (https://creativecommons.org/licenses/by/4.0/).

1. Introduction

Cold forging is widely used in many industries, especially in the manufacturing of fasteners. It is performed at room temperature and requires no further machining to obtain good tolerances, high mechanical properties, and a good surface appearance [1]. Multi-stage cold forging has been widely used to produce axisymmetric parts since the successful development of the multi-stage forging machine [2]. Multi-stage cold forging is a high-speed forming process in which billets are sequentially passed through a multi-station forming machine [3]. This forming process is widely used in the production of various component products, such as bolts, screws, nuts, rivets, and special fasteners. It is also used in the production of automotive parts, such as gear blanks, ball studs, piston pins, spark plug shells, valve spring retainers, transmission shafts, etc. In cold forging, the tools are subjected to relatively high stresses. Prediction of the forming forces and stresses is essential for the design of dies and the selection of machines. The strain distribution of each forming stage is important because it determines the hardness distribution and formability of the part [4]. The strains and stresses are affected by the forming area reduction, die geometry, forming speed, lubrication, workpiece material, and billet size.

There are many studies and analyses on cold forming. Many applications used numerical simulation for the forming design prediction and the simulation parameter settings. By using the 2D finite element method, Altan and Knoerr [5] studied suck-in type extrusion defects, bevel gear forging, stress analysis of forging tools, and multi-stage cold forging operation design. MacCormack and Monaghan [6] proposed a three-stage cold forging process for forming the spline shape at the head of the aerospace fasteners. A combination of extrusion (forward and backward) and forging very complex spline geometries is a complicated process. Insights into the operation are gained through numerical simulations of strain, damage, and flow patterns in all three stages. A multi-stage upsetting method to form a thick and wide flange at the pipe end was developed by Hu and Wang [7]. They analyzed the numerical simulation results and discussed the method of determining the step length. Cho et al. [8] numerically studied the process design of the forward and backward extruded axisymmetric parts for cold forging operations. The forming of numerical simulations agreed with the experimental results. To analyze the formability of a multi-stage forging process, Park et al. [9] applied the FE method to construct a systematic process analysis method for the multi-stage forging of the outer race of constant velocity joints. Ji et al. [10] used the numerical code of DEFORM_2D to investigate the cold-forming mechanism of a five-stage extrusion process of shaft parts that were used in gearboxes. The results illustrated that the cold extrusion of the five-stage process was feasible and the forming rules were obtained. Lee et al. [11] developed a process to cold forge high-strength M8 bolts in 1600 MPa grade, which was based on the softening behavior of fully pearlitic materials with an ultimate tensile strength of 1410 MPa. The manufactured bolts were experimentally confirmed as having a tensile strength of 1600 MPa and a delayed fracture strength. Yang and Lin [12] conducted numerical and experimental studies on two forming modes for the two-stage extrusion forming of AISI 1010 carbon steel. The numerical results for the effective strain distribution were consistent with the hardness distribution tested in the experiment.

In order to meet the needs for higher quality, lower fabricating cost, and fast delivery in automotive fastener production, Chen et al. [13] studied injection forging as a possibility for industrial production of automotive fasteners, owing to its potential to shorten the process chains to cold form complex shape parts. With a focus on reducing the cold-forming forces and improving the dimensional accuracy of the parts, they proposed to improve the process and tool design. For the outer race of a constant velocity joint with six inner ball grooves, Kang and Ku [14] conducted a series of experimental studies on the multi-stage cold-forming process. Spheroidized SCr420H billets were used in the experimental study. While with the proposed multi-stage cold forging process, it was verified that the outer race was well formed and the dimensional accuracy of the cold-formed outer race met the demands. Gontarz and Winiarski [15] proposed a new metal-forming process to produce two-step outer flanges on the hollow parts extruded by a movable sleeve. They applied the new method to bring the end flange of the 6060 aluminum alloy tubular blank. They designed this cold-forming process based on numerical simulations and experiments. The experimental results verified the feasibility of cold forging a two-step flange with a diameter approximately twice the outer diameter of the tubular blank. A two-stage cold-forging process was proposed by Ku [16] for the fabrication of AISI 1035 steel drive shafts with internal spline and spur gear geometry. The process mainly included a forward extrusion of preform and forward and backward extrusion of the drive shaft. The results illustrated that the proposed two-stage cold-forming process may well be applied to fabricate drive shafts with internal spline and spur gear structures. Al-Shammari et al. [17] constructed a six-stage cold-forming process design for the AISI 1010 steel shell of the spark plug fabrication using a 3D geometric model. Numerical analyses were carried out on the product part dimensions, forging loads, effective stresses, contact pressure, and velocity fields. The actual dimensions and forging loads of the product parts at six stages were compared by using the finite element simulation results to verify whether the analysis results were acceptable. Byun et al. [18] conducted a numerical study on the automatic multi-stage

cold-forging of SUS304 stainless steel ball studs. They investigated the plastic deformation behavior of SUS304 stainless steel from room temperature to 400 °C and expressed the flow stress as a closed-form function of the strain, strain rate, and temperature, using a general method. It was optimal at high strains, especially during multi-stage cold forging. Winiarski et al. [19] applied DEFORM 2D/3D to study, numerically, a six-stage cold forging process on the 42CrMo4 steel hollow flanged part to determine whether the proposed forging technique could be used to produce flanged hollow parts. A multi-stage cold-forming process applying finite element analysis was developed by Jo et al. [20] to fabricate a high-strength one-body input shaft with a long body without separate parts. This study demonstrated the design and development of a multi-stage cold-forming process to fabricate a one-body input shaft with better mechanical properties and material recovery. Dubiel et al. [21] introduced the cold forging process of flanged bolts to obtain a consistent, acceptable, and inconsistent grain flow pattern. Then, the FEM simulation results were correlated with the conducted experiments. Szala et al. [22] investigated the hardness behavior and microstructure of 42CrMo4 steel hollow parts with external flanges. Cold forming of metals leads to the work hardening of steels. Metallographic studies verified that flow line arrangement was appropriate, which agreed with that shown by the numerical simulations. The metal forming process did not influence the microstructural uniformity of the flanged hollow parts. The final external flange part demonstrated a high quality that was free of plastic deformation non-uniformity.

Multi-stage cold forging can distribute the forming load and improve dimension accuracy. This study presents the numerical simulation and forming experiments of a five-stage cold-forming process for relief valve regulating nut manufacturing. The forming process included preparation and centering for backward extrusion, backward extrusion over die pin, upset, backward extrusion over moving punch, and piercing. The cold-forming experiments were carried out on a 20-tonne universal testing machine to verify the results of the numerical analysis. The numerical simulation of five-stage cold forming was investigated by using the FE code of DEFORM-3D. Numerical analysis was used to calculate the maximum forming force for each stage and analyze the metal flow pattern, effective stress, and effective strain in various deformation zones.

2. Materials and Methods

The manufacturing process of the relief valve regulating nut was the multi-stage cold forming with five stages. The actual forming machine had five-stage dies. A cold-forging quality AISI 1010 steel wire coil, which was fabricated by China Steel Corporation, Kaohsiung, Taiwan, was used in the cold-forming experiments. The chemical composition of the steel wire is shown in Table 1.

Table 1. Chemical composition of AISI 1010 steel wires (wt.%).

C	Mn	P	S	Si	Al
0.10	0.50	0.021	0.007	0.03	0.035

The cold-forming experiments were conducted using a 20-tonne universal testing machine under a constant ram speed of 5 mm/min at room temperature. A billet of ϕ7.7 mm $\times$ L24.2 mm was cut by the shear die and moved to the next forming stages. The 3D and cross-section views for the initial billet and forming parts of each stage are shown in Figure 1.

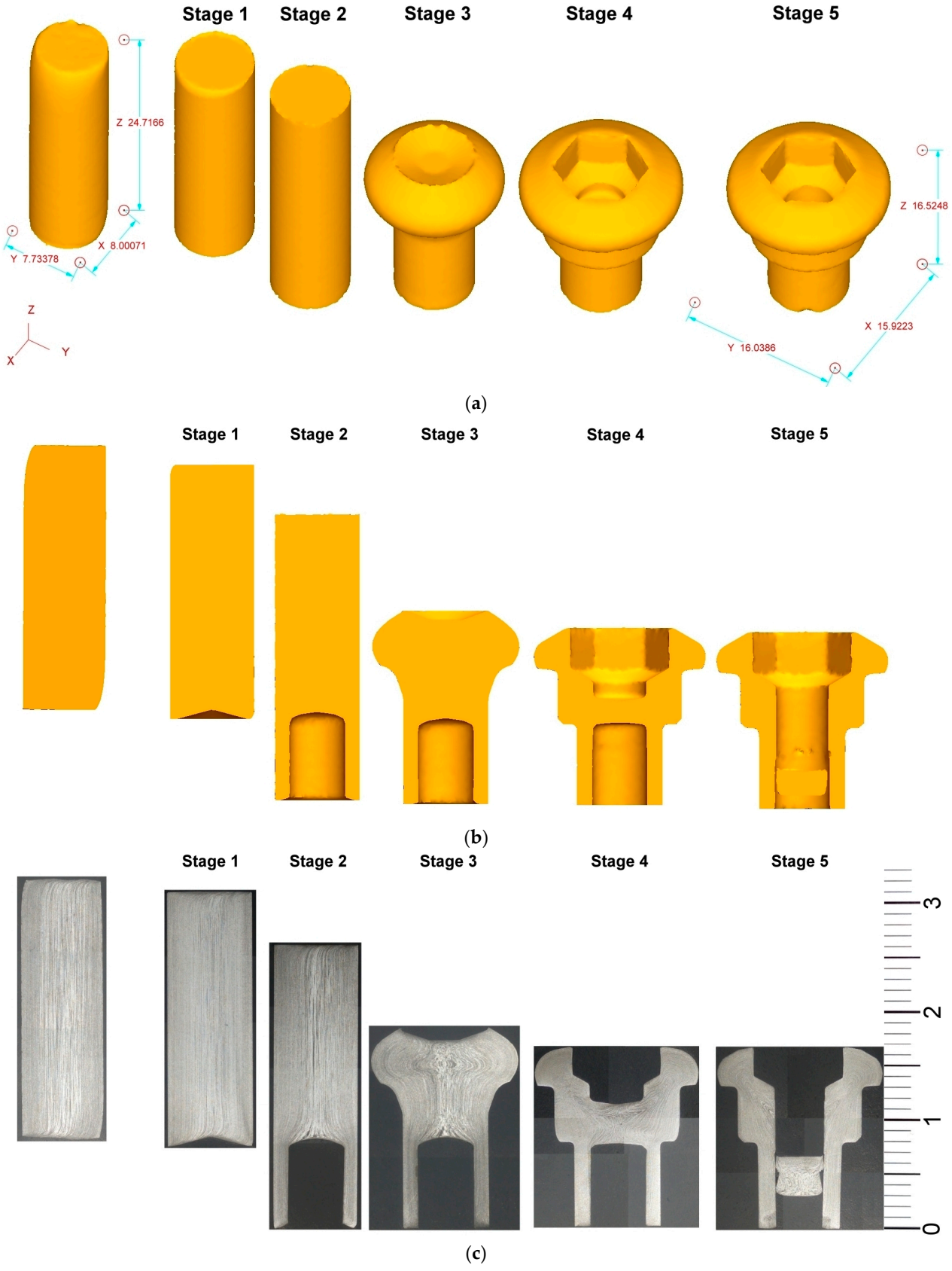


Figure 1. The shapes for initial billet and product parts of five stages. (**a**) 3D views (simulation), (**b**) cross-section views (simulation), (**c**) cross-section views (experiment).

There was visible deformation at the ends of the cutoff billet, as shown in Figure 1, due to it being cut to length by shearing. For the first stage, the preparation process includes flattening the billet end and centering for the backward extrusion, which then moves to the second stage through the transfer mechanism, where the extrusion tool mounted in the die (stationary) conducted the backward extrusion. A cavity of ϕ5.2 mm was formed at the bottom end with a depth of 8.0 mm by using a punch tool mounted in the die and with a reduction in the area of 43.9% for the backward extrusion. Then, the workpiece was delivered to the third stage, where the upper end of the workpiece was upset and prepared for backward extrusion, and delivered to the fourth stage where the backward extrusion over a moving punch formed a hexagonal cavity at the upper face. Finally, it moved to the fifth stage, where the inner hole was formed by piercing. The deformation energy was determined as follows:

$$E = \int_0^{\Delta L} F dl, \tag{1}$$

where F is the forming force and ΔL is the total acted forming stroke.

The numerical simulations of the five-stage cold forming were constructed as 3D finite elements using the DEFORM-3D FE code. The workpiece was constructed using tetrahedral elements. Since the tool materials are generally much harder than the workpiece, their deformations were ignored and considered rigid bodies. The material of the workpiece was an AISI 1010 carbon steel billet, which was treated as a rigid-plastic material, following the Von Misses yield criterion of isotropic hardening. For more accurate simulation results, a cylindrical compression test, with 5 specimens of ϕ7.68 mm × L11 mm (not lubricated at both ends), was performed using a 20-tonne universal testing machine under a constant ram speed of 3 mm/min at room temperature, and the following equations were used to obtain the compression true stress and compression true strain [23]:

$$\sigma = P/A_0, \tag{2}$$

$$\varepsilon = (h - h_0)/h_0, \tag{3}$$

$$\sigma_t = \sigma\,(1 + \varepsilon) = \sigma\,(h/h_0), \tag{4}$$

$$\varepsilon_t = \ln(1 + \varepsilon) = \ln(h/h_0), \tag{5}$$

where σ is the engineering stress, ε is the engineering strain, P is the compression force, A_0 is the initial cross-sectional area, d_0 is the initial diameter, h_0 is the initial height, h is the instantaneous height, σ_t is the compression true stress, and ε_t is the compression true strain. Figure 2 demonstrates the compression true stress–compression true strain diagram of AISI 1010, which was required in the simulation.

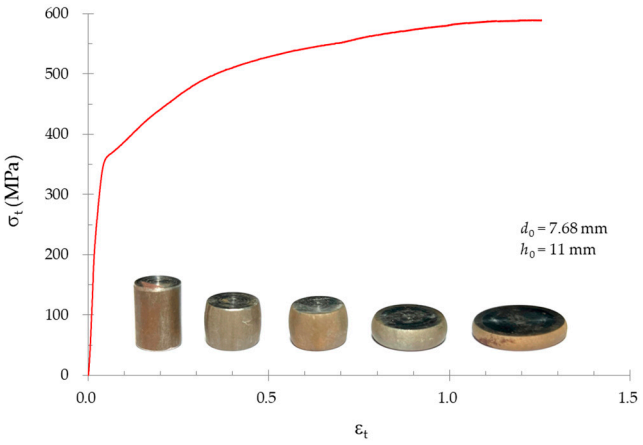


Figure 2. Compression true stress–compression true train curve of AISI 1010 using the compression test at room temperature.

For cold forming, the constant shear friction was considered as the friction between the workpiece and the tools using a friction coefficient of m = 0.12. The relevant simulation settings are listed in Table 2.

Table 2. Simulation settings in the FE code of DEFORM.

Workpiece Material	**AISI 1010**
Workpiece/die property	Plastic/rigid
Temperature	20 °C
Mesh number	75,000
Mesh element type	Tetrahedron
Friction model/friction coefficient	Constant shear friction/0.12

3. Results and Discussion

For the multi-stage cold forming of the relief valve regulating nut through five stages, the effect of forming force response, maximum forming force, effective stress and effective strain distributions, metal flow pattern, and strength were investigated both numerically and experimentally.

3.1. The Forming Force and Deformation Energy

A comparison of the forming forces recorded in the forming experiments with the five-stage forming simulation results is shown in Figure 3. It indicates a good agreement in the forming force responses. The numerical and experimental maximum forming forces are indicated for each stage. The forming stroke and deformation energy for each stage are displayed in Table 3. For the forming forces, as illustrated in Figure 3, the maximum forming forces in the forming experiment and numerical simulation of each stage are very close.

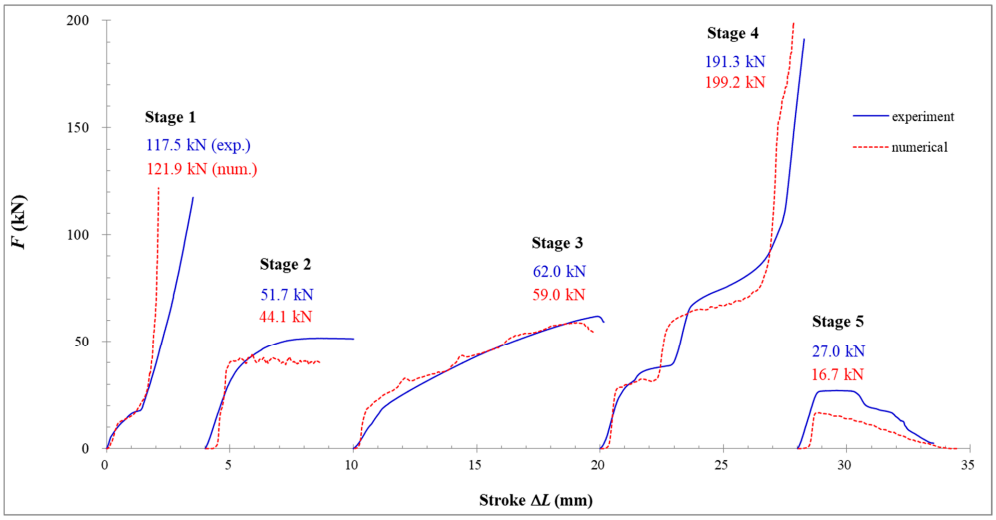


Figure 3. Forming forces versus stroke for five stages.

Table 3. The acted forming stroke (ΔL) and deformation energy (E) for each stage.

	Stage	**1**	**2**	**3**	**4**	**5**	**Total**
Experiment	E (J)	147.5	256.1	410.9	548.8	95.0	1458.4
	ΔL (mm)	3.51	6.01	10.16	8.27	5.52	
Numerical	E (J)	47.3	164.5	407.7	504.0	50.1	1173.6
	ΔL (mm)	2.11	4.71	9.81	7.85	6.52	

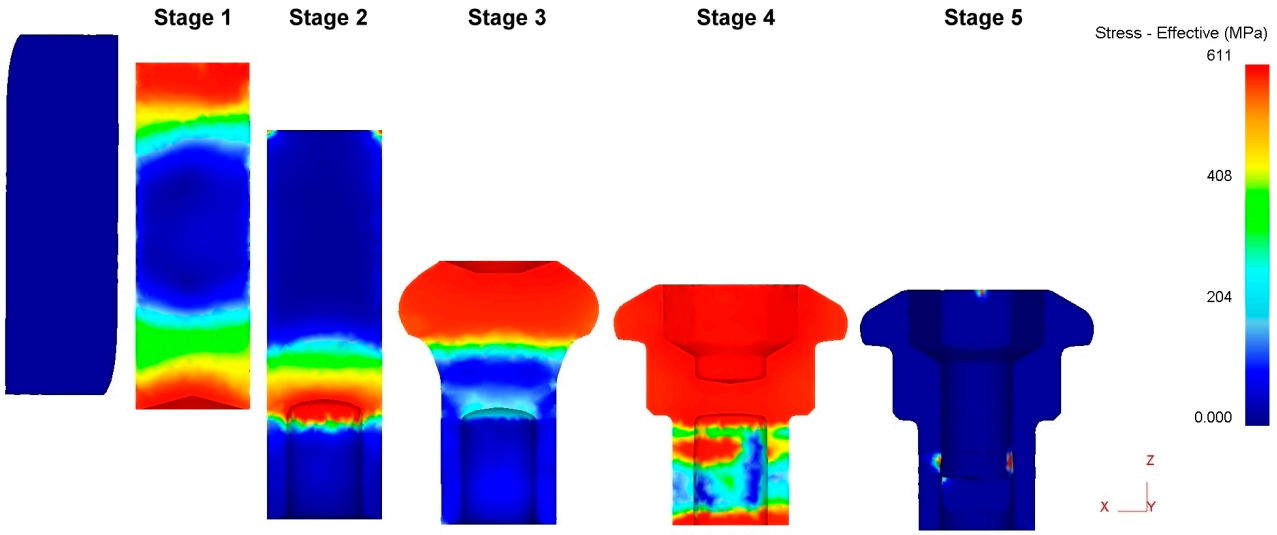
From the force responses of the forming force in the five stages, it was observed that at the first stage, the maximum forming forces were 121.9 kN numerically and 117.5 kN experimentally. There was only a minor deformation to remove the sharp cutting edges and to center for the backward extrusion. In the second stage, the maximum forming forces increased to 44.1 kN (num.) and 51.7 kN (exp.) for the backward extrusion over the die pin, with a reduction in area of 43.9% to form the cavity of ϕ5.2 mm with an 8.0 mm depth. In the third stage, the maximum forming forces increased to 59.0 kN (num.) and 62.0 kN (exp.) to upset a head. For the forming force response, the numerical simulation was in good agreement with the experimental result, as shown in Figure 3, and the forming energies of 407.7 J (num.) and 410.9 J (exp.) were also relatively close (0.8% error), as shown in Table 3. In the fourth stage, a backward extrusion process was performed by moving the punch to form a hexagonal cavity at the upper end, which included a complicated cavity shape, meaning high pressure was required to force the material to complete the die cavity filling. The maximum forming forces were increased to 199.2 kN (num.) and 191.3 kN (exp.) The increasing of the forming force to fully form the metal into the shape of the cavity could potentially lead to the wear and failure of the die. For the forming force response, the numerical simulations agreed with the experimental results, as shown in Figure 3. The forming energies of 504.0 J (num.) and 548.8 J (exp.) were also close (8.2% error), as shown in Table 3. At the last stage, the maximum forming forces were 16.7 kN (num.) and 27.0 kN (exp.) to pierce the hole, which were less than at the other stage loads.

For the maximum forming force, as shown in Figure 3, the fourth stage, which was backward extrusion over the moving punch at the upper face (Figure 1), was the largest among the five stages, and the first stage, which was preparation and centering (Figure 1), was the second largest. For the forming energy, as shown in Table 3, the fourth stage was also the largest among the five stages, while the third stage, which was upsetting the upper head (Figure 1) with the largest acted forming stroke, was the second largest. Overall, the total maximum forming forces from the first to the fifth stages were 440.9 kN numerically and 449.4 kN experimentally, and the total forming energies were about 1.174 kJ (num.) and 1.458 kJ (exp.). The FE simulation and experimental results are in good agreement.

3.2. The Effective Stress Analysis

The effective stress distributions are shown in Figure 4 for the final position of each stage, and the maximum effective stresses are indicated. In the first stage, when the billet was contacted with the dies, the stresses are generated at the upper and lower ends, then, the stresses increased as the forming force increased, and the maximum effective stress was 609 MPa. It was observed that the highest effective stress arose at the upper and lower ends of the workpiece, while the lowest effective stress arose in the middle zone of the workpiece. For the second stage, which involved the backward extrusion over the die pin, it was analyzed from Figure 4 that the effective stresses were high in the extrusion deformation region. This resulted in the formation of a cavity at the lower end, which caused high pressure to arise and an effective stress of up to 609 MPa on the workpiece and tool surface.

In the third stage, the upper end of the workpiece was upset. When the stroke of the punch increased, the upper end of the workpiece was gradually upset. The stress response was obviously large in the upsetting region of the workpiece. The maximum effective stress was 611 MPa. In the fourth stage, the process of backward extrusion over the moving punch was carried out to form a hexagonal cavity. This resulted in the formation of the hexagonal cavity in the upper face being under high pressure and resulted in a highly effective stress of 611 MPa. The stress response of the overall extrusion region of the workpiece was obviously large. The fifth stage was to pierce a hole in the inner cavity, therefore, the stress response was relatively large in the piercing zone of the workpiece. The maximum effective stress was 610 MPa.



Max. (MPa)	609	609	611	611	610

Figure 4. The effective stress distributions at the final position for five stages.

3.3. The Effective Strain Analysis

Figure 5 shows the effective strain distributions at the final position for each stage.

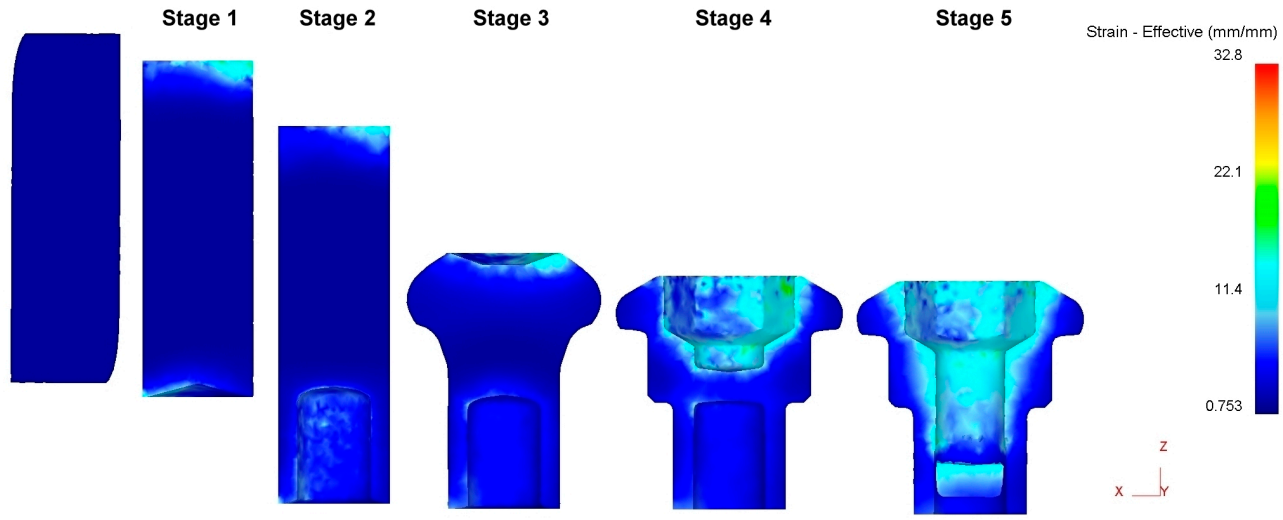


Figure 5. The effective strain distributions at the final position for five stages.

In the first stage, the effective strains in the flatting (upper) and centering (lower) regions of the workpiece were larger than in the middle region where the deformation was small, as illustrated in Figure 5, while the effective strain distributions were not perfectly symmetrical because of the visible deformation at the ends of the cutoff billet. For the second stage of the backward extrusion over a die pin, the effective strains both in the upper end and the region of backward extrusion with large deformation were large. Due to the friction resistance on the contact surface between the die pin and the workpiece, the effective strains along the die pin region increased evidently, and the material flow was also less uniform. For the third stage, the upsetting of the upper end of the workpiece, the effective strains were obviously high in the upsetting zone, while the effective strains of the other region were relatively small. In the fourth stage of the backward extrusion over moving punch to form a hexagonal cavity, the effective strains in the overall region of the backward extrusion with large deformation were evidently large, as shown in Figure 5.

In the fifth stage, where a hole was formed by a piercing punch in the internal cavity, the highly effective strains were distributed in the inner wall of the hole and the piercing waste, as shown in Figure 5.

3.4. The Hardness Analysis

During cold forging, the hardness and strength of the workpiece may increase due to the plastic flow. Figure 6 shows the average hardness (measured in Vickers hardness) of the workpiece cross-section at each stage by experiment. The red dot in the Figure is the position where the maximum hardness was measured. The hardness of the initial billet was almost the same and evenly distributed (about 142 HV), as shown in Figure 6, except for the higher hardness at both ends (about 173 and 194 HV) due to shear deformation. The average hardness overall of the initial billet was 158.6 HV.

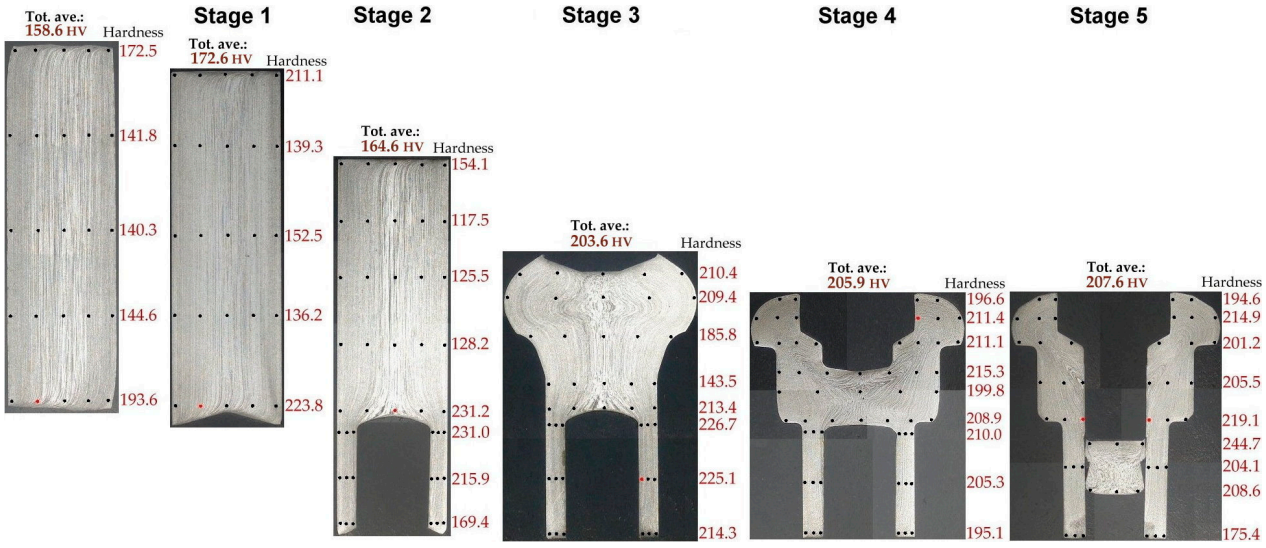


Figure 6. The hardness (in HV) and gran flow lines in workpieces for five stages.

In the first stage, the hardness of the flatting and centering zones of the workpiece was larger than in the middle zone where the deformation was small, which was consistent with the effective strain distribution in Figure 5. The overall hardness of the workpiece (172.6 HV in average) was greater than the initial billet. The highest hardness of 247.6 HV was inspected in the bottom cross-section of the workpiece due to the centered forming.

For the second stage of the backward extrusion over the die pin, the hardness in the upper end and the region of the backward extrusion forming was greater than in the middle region, which agreed with the effective strain distributions shown in Figure 5. The hardness distribution in the workpiece was relatively uneven, as shown in Figure 6. The hardness distribution around the inner wall of the lower cavity was obviously high (approx. 250 HV in average) due to the severe structure deformation. The average hardness overall the workpiece was 164.6 HV. The highest hardness was 290.9 HV, which was identified at the center of the section, immediately above the lower cavity of the workpiece, indicated by the red dot in Figure 6, due to the large plastic flow of the backward extrusion forming.

In the third stage, the hardness in the upsetting zone of the workpiece, where the higher distribution of the effective strain is shown in Figure 5, was higher than in the middle region. The hardness distribution around the inner wall of the lower cavity, formed by the previous stage, remained high (approx. 248 HV in average). The overall hardness in the workpiece (203.6 HV in average) was greater than the initial billet and the previous two stages. The highest hardness was 290.9 HV, which was identified in the middle section of the thin wall, shown by the red dot in Figure 6.

For the fourth stage of the backward extrusion over the moving punch to form a hexagonal cavity, the hardness in the backward extrusion forming zone was obviously

higher, as shown in Figure 6. Due to the large amount of extrusion, the hardness in the extruded inner wall area was relatively large (about 222 HV in average), and a higher distribution of effective strain was also shown in Figure 5. The highest hardness was 264.2 HV, which was observed closest to the inner wall of the second section from the top of the workpiece (red dot in Figure 6). The overall hardness in the workpiece was averaged at around 205.9 HV, which was larger than the initial billet and the previous three stages, while the difference from the third stage was relatively small.

In the fifth stage, the piercing of a hole in the internal cavity, the high hardness was distributed around the inner wall of the hole and in the piercing waste, as shown in Figure 6. The hardness around the inner wall of the hole was relatively large (about 240 HV in average), which agreed with the effective strain distributions shown in Figure 5. The highest hardness was 266.7 HV, which was observed closest to the inner wall of the middle section of the workpiece (red dots in Figure 6). The overall hardness of the workpiece (207.6 HV in average) was the highest among the five stages, increasing by 31% compared to the initial billet. The hardness of the workpiece increased with the forming stages, and the strain-hardening effect was obvious. The work hardening of the steel is often caused by cold forming.

The strength of the workpiece formed by five-stage cold forming was obviously greater than for the initial billet. If the workpiece was no longer heat-treated, this effect may be applied to replace medium carbon or alloy steels with low carbon steels.

3.5. The Flow Line Analysis

Grain flow is evident when inspecting the interior of the forging. When the metal was deformed by cold forging, the deformed grains and inclusions are distributed in bands along the main elongation direction of the metal to form the grain flow lines. Figure 6 shows, experimentally, the grain flow lines of the workpieces for each stage, and the simulation results of the flow lines for the five stages are shown in Figure 7. A comparison between the simulated results and those revealed by metallographic investigations in Figure 6 indicated a similar flow line arrangement.

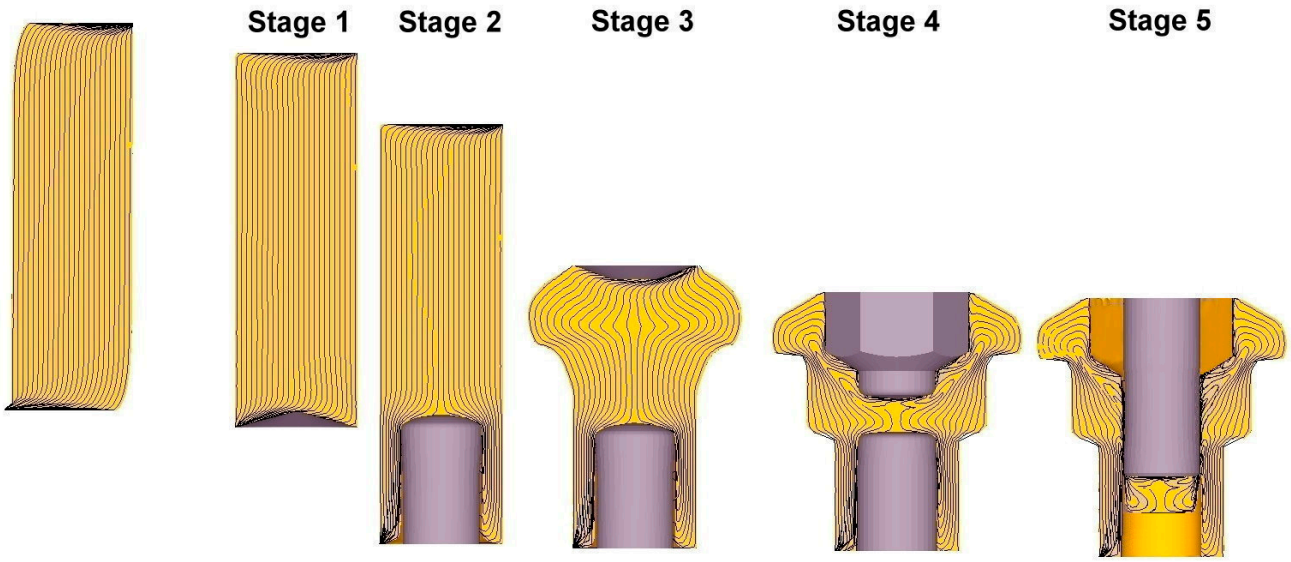


Figure 7. The simulation results of flow lines at the final position for five stages.

The flow lines in the initial billet were almost evenly distributed, as shown in Figures 6 and 7, except at both ends where, due to shear deformation, the flow lines were bent by 90 degrees and highly compacted. Highly compacted flow lines also resulted in a higher hardness, as shown in Figure 6.

In the first stage, the flow lines in the flatting and centering regions of the workpiece were highly compacted, while in the middle region with low deformation, the flow lines were almost evenly distributed. The hardness was relatively small, as shown in Figure 6. For the second stage of the backward extrusion over a die pin, the flow lines in the inner wall of the lower cavity were obviously highly compacted due to the severe structure deformation. The hardness was relatively high, as shown in Figure 6. In the third stage, the flow lines in the upsetting zone of the workpiece were heavily curved and highly compacted, as shown in Figures 6 and 7. The hardness was obviously higher. For the fourth stage of the backward extrusion over the moving punch to form a hexagonal cavity, the flow lines were more severely curved and highly compacted in the zone of the backward extrusion forming, as shown in Figures 6 and 7, the hardness was also relatively higher. In the fifth stage, the piercing of a hole in the internal cavity, the forging flow lines around the inner wall of the hole were deformed to be more compacted and eventually broke. Therefore, the hardness was also relatively high in the zone around the inner wall of the hole and in the piercing waste, as illustrated in Figure 6.

4. Conclusions

In this study, a multi-stage cold-forming process for the manufacturing of relief valve regulating nuts was carried out both numerically and experimentally. The forming process through five stages included the preparation and centering for backward extrusion, backward extrusion over a die pin, upsetting, backward extrusion over the moving punch, and piercing. The cold-forming experiments were carried out on a 20-tonne universal testing machine using the designed forming dies. The finite element code of DEFORM-3D was used for the numerical simulation analysis of the five-stage cold forming. The formability of the workpiece was investigated, such as the effect on the forming force response, maximum forming force, effective stress and effective strain distribution, metal flow patterns, and strength.

A comparison between the forming forces obtained in the forming experiment and the numerical simulation results for the five-stage cold forming shows that the forming force responses are in good agreement. For the maximum forming force and forming energy, the fourth stage of the backward extrusion over the moving punch at the upper face was the largest among the five stages. The total maximum forming forces from the first to the fifth stages were numerically 440.9 kN and experimentally 449.4 kN, and the total forming energies were numerically about 1.174 kJ and experimentally about 1.458 kJ. The numerical simulations and experimental results were in good agreement. The numerically simulated effective strain distributions were consistent with the experimentally tested hardness distribution. Highly compacted grain flow lines also resulted in higher hardness. The overall hardness of the workpiece (average 207.6 HV) formed by five-stage cold forming increased by 31% compared to the initial billet. The hardness of the workpiece increased with the forming stages, and the strain-hardening effect was obvious. The strength of the workpiece was significantly increased by the five-stage cold forming. This effect can be applied to replace medium carbon or alloy steels with low carbon steels if not heat treated. This study provides an effective reference for designers.

Author Contributions: Conceptualization, C.-C.Y. and C.-H.L.; methodology, C.-C.Y.; validation, C.-C.Y.; investigation, C.-C.Y. and C.-H.L.; resources, C.-H.L.; data curation, C.-H.L.; writing—original draft preparation, C.-C.Y.; writing—review and editing, C.-C.Y. All authors have read and agreed to the published version of the manuscript.

Funding: This research received no external funding.

Institutional Review Board Statement: No applicable.

Informed Consent Statement: No applicable.

Data Availability Statement: No new data were created or analyzed in this study. Data sharing is not applicable to this article.

Acknowledgments: The authors would like to acknowledge the support of Jie Shuen Industrial Co., Ltd., Kaohsiung, Taiwan, for providing the materials to carry out the forming experimental work.

Conflicts of Interest: The authors declare no conflict of interest.

References

1. Wagoner, R.H.; Chenot, J.-L. *Metal Forming Analysis*; Cambridge University: Cambridge, UK, 2001.
2. Sevenler, K.; Raghupati, P.S.; Altan, T. Forming Sequence Design for Multi-stage Cold Forging. *J. Mech. Work. Technol.* **1987**, *14*, 121–135. [CrossRef]
3. Padfield, T.; Bhupatiraju, M. Cold heading. In *Metalworking: Bulk Forming*; ASM International: Materials Park, OH, USA, 2008.
4. Kobayashi, S.; Oh, S.-I.; Altan, T. *Metal Forming and the Finite-Element Method*; Oxford University: Oxford, UK, 1989.
5. Altan, T.; Knoerr, M. Application of the 2D Finite Element Method to Simulation of Cold Forging Processes. *J. Mater. Process. Technol.* **1992**, *35*, 275–302. [CrossRef]
6. MacCormack, C.; Monaghan, J. 2D and 3D finite element analysis of a three stage forging sequence. *J. Mater. Process. Technol.* **2002**, *127*, 48–56. [CrossRef]
7. Hu, X.L.; Wang, Z.R. Numerical simulation and experimental study on the multi-step upsetting of a thick and wide flange on the end of a pipe. *J. Mater. Process. Technol.* **2004**, *151*, 321–327. [CrossRef]
8. Cho, H.Y.; Min, G.S.; Jo, C.Y.; Kim, M.H. Process design of the cold forging of a billet by forward and backward extrusion. *J. Mater. Process. Technol.* **2003**, *135*, 375–381. [CrossRef]
9. Park, K.S.; VanTyne, C.J.; Moon, Y.H. Process analysis of multistage forging by using finite element method. *J. Mater. Process. Technol.* **2007**, *187*, 586–590. [CrossRef]
10. Ji, D.S.; Jin, J.S.; Ma, W.J.; Xia, J.C.; Xia, H.G.; Dong, Y. Multistage Cold Extrusion Process and Forming Rules of Shaft Parts Used in Gearbox. *Adv. Mater. Res.* **2010**, *148*, 683–687. [CrossRef]
11. Lee, H.C.; Jin, Y.G.; Lee, Y.H.; Son, I.H.; Lee, D.L.; Im, Y.T. Process Design of High-strength Bolt of Fully Pearlitic High-carbon Steel. *J. Mater. Process. Technol.* **2010**, *210*, 1870–1875. [CrossRef]
12. Yang, C.-C.; Lin, X.-Y. The Forming Analysis of Two-stage Extrusion for 1010 Fastener. *J. Mech. Eng. Autom.* **2016**, *6*, 43–45.
13. Chen, S.; Qin, Y.; Choy, C.-M.; Chen, J.G. Testing an injection forging process for the production of automotive fasteners. *Procedia Eng.* **2017**, *207*, 508–513. [CrossRef]
14. Kang, B.S.; Ku, T.W. Experimental Study on Multi-Stage Cold Forging for an Outer Race of a CV Joint. *Trans. Mater. Process.* **2014**, *23*, 221–230. [CrossRef]
15. Gontarz, A.; Winiarski, G. Numerical and Experimental Study of Producing Two-Step Flanges by Extrusion with a Movable Sleeve. *Arch. Metall. Mater.* **2017**, *62*, 495–499.
16. Ku, T.-W. A Study on Two-Stage Cold Forging for a Drive Shaft with Internal Spline and Spur Gear Geometries. *Metals* **2018**, *8*, 953. [CrossRef]
17. Al-Shammari, M.A.; Zedan, L.Y.; Al-Shammari, A.M. FE simulation of multi-stage cold forging process for metal shell of spark plug manufacturing. In Proceedings of the 2018 1st International Scientific Conference of Engineering Sciences—3rd Scientific Conference of Engineering Science (ISCES), Diyala, Iraq, 10–11 January 2018.
18. Byun, J.B.; Razali, M.K.; Lee, C.J.; Seo, I.D.; Chung, W.J.; Joun, M.S. Automatic Multi-Stage Cold Forging of an SUS304 Ball-Stud with a Hexagonal Hole at One End. *Materials* **2020**, *13*, 5300. [CrossRef] [PubMed]
19. Winiarski, G.; Bulzak, T.A.; Wójcik, Ł.; Szala, M. Numerical Analysis of a Six Stage Forging Process for Producing Hollow Flanged Parts from Tubular Blanks. *Adv. Sci. Technol. Res. J.* **2020**, *14*, 201–208. [CrossRef]
20. Jo, A.R.; Jeong, M.S.; Lee, S.K.; Moon, Y.H.; Hwang, S.K. Multi-Stage Cold Forging Process for Manufacturing a High-Strength One-Body Input Shaft. *Materials* **2021**, *14*, 532. [CrossRef] [PubMed]
21. Dubiel, T.; Balawender, T.; Osetek, M. The Fibrous Structure of the Bolt and Its Effect on the Joint Reliability. *Arch. Metall. Mater.* **2021**, *66*, 1075–1085.
22. Szala, M.; Winiarski, G.; Bulzak, T.; Wójcik, Ł. Microstructure and Hardness of Cold Forged 42CrMo4 Steel Hollow Component with the Outer Flange. *Adv. Sci. Technol. Res. J.* **2022**, *16*, 201–210. [CrossRef]
23. Hosford, W.F. *Mechanical Behavior of Materials*; Cambridge University: Cambridge, UK, 2005.

Disclaimer/Publisher's Note: The statements, opinions and data contained in all publications are solely those of the individual author(s) and contributor(s) and not of MDPI and/or the editor(s). MDPI and/or the editor(s) disclaim responsibility for any injury to people or property resulting from any ideas, methods, instructions or products referred to in the content.